ELSEVIER

Journal of Organometallic Chemistry 553 (1998) 15–22

Journal of Organometallic Chemistry

Synthesis and crystal structure of a zirconium(III) diacetylide tweezer complex: $[(\eta^5\text{-}C_5HMe_4)_2Zr(\eta^1\text{-}C{\equiv}CSiMe_3)_2]^-K^+$

Vojtech Varga [a], Jörg Hiller [b], Ulf Thewalt [b], Miroslav Polášek [a], Karel Mach [a,*]

[a] *J. Heyrovský Institute of Physical Chemistry, Academy of Sciences of the Czech Republic, Dolejškova 3, 182 23 Prague 8, Czech Republic*
[b] *Sektion für Röntgen- und Elektronenbeugung, Universität Ulm, D-89069 Ulm, Germany*

Received 27 December 1996

Abstract

The zirconocene diacetylide $(\eta^5\text{-}C_5HMe_4)_2Zr(\eta^1\text{-}C{\equiv}CSiMe_3)_2$ (**1**) is reduced by potassium in toluene to give the paramagnetic tweezer complex $[(\eta^5\text{-}C_5HMe_4)_2Zr(\eta^1\text{-}C{\equiv}CSiMe_3)_2]^-K^+$ (**2**). The presence of Zr(III) follows from the ESR spectrum of **2** ($g = 1.9914$, $a_{Zr} = 1.86$ mT). The X-ray crystal structures show that the bite angle of tweezer arms of 102.7° in **1** is diminished to 92.8° in complex **2**. The potassium cation is embedded between the acetylide arms, 1.13 Å away from the bite angle plane, at the Zr-K distance of 3.818(1) Å.

1. Introduction

In contrast to numerous Zr(IV) complexes, monomeric Zr(III) complexes are scarcely reported, with most of the evidence being drawn from ESR spectra of reacting systems of Zr(IV) derivatives reduced by chemical agents or electrochemically [1]. The X-ray crystal structures were reported only for the following paramagnetic Zr(III) compounds: $(\eta\text{-}C_5(1,3\text{-}^tBu)_2H_3)_2ZrCl$[2], $(\eta\text{-}C_5Me_5)(\eta\text{-}C_8H_8)Zr$ [3], (OEP)$ZrCH_2SiMe_3$ (OEP = octa-ethylporphyrin) [4], $(\eta\text{-}C_5H_5)$(Ph)$Zr[N(SiMe_2CH_2P^iPr_2)_2]$ and $(\eta\text{-}C_5H_5)(CH_2SiMe_3)Zr[N(SiMe_2CH_2P^iPr_2)_2]$ [5]. In contrast to the dimers of Ti(III) compounds which are largely paramagnetic [6], forming the triplet state, the dimers of Zr(III) compounds are diamagnetic [1,7] except the poorly characterized complex $[(C_5H_5)_2ZrCH(SiMe_3)_2]_2(\mu\text{-}N{\equiv}N)$ [8]. The 1,3-bis(trimethylsilyl)cyclopentadienyl zirconocene monohalides are also dimers bridged by $(\mu\text{-}Cl)_2$, $(\mu\text{-}Br)_2$ and $(\mu\text{-}I)_2$ elements, although with extra long Zr-Zr distances (av. 3.90 Å, 4.10 Å, and 4.17 Å respectively). The chloro complex, however, undergoes a nucleophilic bridge cleavage addition with $[NBu_4]Cl$ or $[Li(THF)_n][1,2\text{-}\{P(SiMe_3)_2\}_2C_6H_4]$ to give stable zirconocenate(III) complexes [9].

Here we report the synthesis and X-ray structure of another zirconocenate(III) complex, $[(\eta_5\text{-}C_5HMe_4)_2Zr(\eta^1\text{-}C{\equiv}CSiMe_3)_2]^-K^+$ (**2**), a paramagnetic zirconocene(III) diacetylide complex of the tweezer type. The preparation and the structure of its Zr(IV) precursor $(\eta^5\text{-}C_5HMe_4)_2Zr(\eta^1\text{-}C{\equiv}CSiMe_3)_2$ (**1**) are also described.

2. Experimental details

All manipulations with reagents, the synthesis, and most of spectroscopic measurements were carried out under vacuum using all-sealed glass devices equipped with breakable seals.

2.1. Chemicals

The solvents toluene and hexane were dried by refluxing over $LiAlH_4$ and stored as solutions of the dimeric titanocene $(C_{10}H_8)[(C_5H_5)Ti(\mu\text{-}H)]_2$ [10]. Butyllithium (BuLi) in hexane (1.6 M) was obtained from Aldrich. Trimethylsilylethyne (Aldrich) was degassed and distilled onto a small amount of dimeric titanocene. After standing overnight the solution was degassed and trimethylsilylethyne was distilled into a

* Corresponding author.

storage ampoule under metal valve. $(C_5HMe_4)_2ZrCl_2$ was prepared as described elsewhere [11].

2.2. Methods

ESR spectra were recorded on an ERS-220 spectrometer (Centre for Production of Scientific Instruments, Academy of Sciences, Berlin, Germany) in the X-band; *g*-values were determined using an Mn^{2+} ($M_1 = -1/2$ line) standard at $g = 1.9860$ and a proton magnetometer MJ-110 R (Radiopan, Poznan, Poland). Concentrations of the paramagnetic compounds were estimated from integrated first derivation spectra. An STT-3 variable-temperature unit was used for measurements in the range -140 to +20 °C. Samples were measured as solutions in hexane, THF, toluene and MTHF. The toluene and MTHF solutions were used for the measurement of anisotropic spectra in frozen organic glasses. UV-vis spectra in the range 280-2000 nm were obtained on a Varian Cary 17D spectrometer using all-sealed quartz cuvettes (Hellma). Mass spectra were measured on a Jeol D-100 spectrometer at 70 eV (only important mass peaks and peaks of intensity not below 5% are reported). Samples in capillaries were opened and inserted into the direct inlet under argon. Infrared spectra of hexane or toluene solutions were recorded on a UR-75 instrument (Zeiss, Jena, Germany) using KBr cuvettes filled under argon. KBr pellets of crystalline **1** and **2** were prepared in a glovebox Labmaster 130 (mBraun) under purified nitrogen and were measured in an air-protecting cuvette on a Mattson Galaxy 2020 IR spectrometer. ^1H and ^{13}C NMR spectra of **1** were measured on a Varian VXR-400 spectrometer (400 MHz and 100 MHz respectively) in C_6D_6 at 25 °C. Samples were referenced to residual benzene as internal standard (δ_H 7.15 and δ_C 128.00 ppm). Electron dispersive X-ray (EDX) analyses were carried out on a Zeiss DSM-962 scanning electron microscope equipped with an EDAX PV9800 analyser. An acceleration voltage of 25 kV was used. Melting points were determined in sealed glass capillaries under nitrogen, and are uncorrected.

2.3. Preparation of $(\eta^5\text{-}C_5HMe_4)_2Zr(\eta^1\text{-}C{\equiv}CSiMe_3)_2$ **1**

A solution of *n*-BuLi (1.6 M, 2.5 ml) was added to trimethylsilylethyne (0.6 ml, 4 mmol) in 40 ml of hexane. After stirring for 1 h at room temperature all volatiles were removed under vacuum and the white residue of $LiC{\equiv}CSiMe_3$ [12] was dissolved in 40 ml of toluene. This solution was added to $(C_5HMe_4)_2ZrCl_2$ (0.81 g, 2 mmol) in toluene (30 ml). The reaction mix-

Table 1
Crystallographic data and experimental details for **1** and **2**

Compound	**1**	**2**
Crystal data		
Chemical formula	$C_{28}H_{44}Si_2Zr$	$C_{28}H_{44}KSi_2Zr$
Mol. wt. ($g\,mol^{-1}$)	528.03	567.13
Crystal system	monoclinic	triclinic
Space group	$P2_1/c$, No. 14	$P\bar{1}$, No. 2
a (Å)	10.2946(8)	8.0735(9)
b (Å)	19.5216(10)	11.866(2)
c (Å)	15.5205(11)	18.141(2)
α (deg)	90	106.054(9)
β (deg)	91.670(7)	96.802(9)
γ (deg)	90	104.582(12)
Z	4	2
Volume ($Å^3$)	3117.8(4)	1583.0(3)
$D_{calc.}$ ($g\,cm^{-3}$)	1.125	1.190
μ(Mo Kα) (cm^{-1})	4.41	5.67
Crystal size (mm^3)	$0.8 \times 0.7 \times 0.6$	$0.4 \times 0.3 \times 0.3$
Data collection and refinement		
θ range (deg)	3.14–25.02	3.03–25.00
Index ranges	$-12 \le h \le 12$, $0 \le k \le 23$, $0 \le l \le 18$	$-9 \le h \le 9$, $-14 < k < 13$, $0 \le l \le 21$
Total data	5505	5561
Unique data, R_{int}	5505, 0.000	5561, 0.000
No. of parameters	298	291
Goodness-of-fit on F^2	1.188	1.026
$R1$, $wR2$ [$I > 2\sigma(I)$]	0.0576, 0.1243	0.0377, 0.0874
$R1$, $wR2$ (all data)	0.0719, 0.1339	0.0995, 0.1078
Largest dif. peak and hole ($e\,Å^{-3}$)	0.600, −0.418	0.330, −0.369

ture was stirred at 60 °C for 24 h. The toluene was evaporated under vacuum and the residue was extracted by hexane to give a yellow-brown solution. This was separated from a white precipitate of LiCl and its volume was reduced to 20 ml. Cooling to -15 °C overnight afforded a yellow crystalline product. This was recrystallized from hexane in order to reduce the amount of a paramagnetic impurity characterized by EPR parameters $g = 1.9965$, $\Delta H = 3$ G, $a_{Zr} = 35.8$ G. Fine yellow crystals of **1** (0.76 g, 72% yield), m.p. 112 °C. Anal. Found: C, 63.4; H, 8.6. $C_{28}H_{44}Si_2Zr$. Calc.: C, 63.7; H, 8.4%. EDX: Si (Kα), Zr (Lα); UV-vis (hexane)(nm): 365($\log\epsilon \sim 3$). IR (KBr)(cm^{-1}): 3079 (vw), 2957 (s), 2909 (s), 2027 (m), 1499 (vw), 1478 (w), 1451 (m), 1431 (m), 1381 (m), 1370 (m), 1244 (s), 1148 (w), 1026 (m), 856 (vs), 843 (vs), 756 (m), 679 (vs), 606 (m); IR (hexane)(cm^{-1}): ν(C≡C) 2022. ^{1}H NMR (C_6D_6): δ 0.17 (18 H, s, 2 × $SiMe_3$), 1.86 (12 H, s, 4 × Me), 2.23 (12 H, s, 4 × Me), 5.04 (2 H, s, H(Cp)). ^{13}C NMR (C_6D_6): δ 0.6 (6 C, q), 13.4 (4 C, q, 2 × 1-Me, 2 × 4-Me), 14.3 (4 C, q, 2 × 2-Me, 2 × 3-Me), 106.6 (2 C, d, 2 × C-5), 119.7 4 C, s, 2 × C-1, 2 × C-4), 126.0 (2 C, s, 2 × C-α), 127.6 (4 C, s, 2 × C-2, 2 × C-3), 173.3 (2 C, s, 2 × C-β). The assignment is based on proton-coupled ^{13}C NMR spectrum: C-α is a pure singlet; 1-Me has a larger coupling to H-5 than 2-Me (J 1.6 Hz vs. 1.0 Hz); the signal of C-2 is broader than that of C-1 (vicinal vs. geminal coupling to H-5). EI-MS (direct inlet, 50-80 °C): m/z 526 (M^+, 11%), 366(8), 332(100), 209(8), 83(32), 73(5); elemental analysis: 526.1991, error $+3.4 \times 10^{-3}$ for $C_{28}H_{44}Si_2Zr$; 332.1039, error $+3.9 \times 10^{-3}$ for $C_{18}H_{26}Zr$.

2.4. Preparation of $[(\eta^5\text{-}C_5HMe_4)_2Zr(\eta^1\text{-}C{\equiv}CSiMe_3)_2]^-K^+$ (2)

Compound **1** (0.45 g, 0.85 mmol) was dissolved in toluene (10 ml) and the solution was added to freshly cut pieces of potassium (0.27 g, 7 mmol) in vacuo. The mixture was gently stirred by glass-coated magnetic stirrer bar for 4 h at room temperature. During this time the nearly colourless solution turned through brown to deep red-brown. The complete consumption of **1** was proven by the absence of its band at 2022 cm^{-1} in the IR spectrum of the probe separated from the reaction solution. The reaction solution was then separated from unreacted potassium and was evaporated under vacuum. The residue was washed with three portions of hexane (10 ml) to remove a trace of **1** and the paramagnetic impurity which was present already in **1** (see above). The brown solid residue was dissolved in toluene to give a brown solution. Slow evaporation of the solvent afforded dark green crystals of compound **2** (yield 0.42 g, 87%), m.p. 243 °C. Anal. Found: C, 59.1; H, 7.9. $C_{28}H_{44}KSi_2Zr$. Calc.: C, 59.3; H, 7.8%. EDX: Si, K (Kα), Zr (Lα); UV-vis (toluene, dark yellow)(nm): 580(sh) ≪ 440 > 383 > 315, 305; (MTHF, dark yellow)(nm): 550(sh) ≪ 440 > 380 > [315, 305, 288, 270 (sharp bands, vibronic structure)]. IR (KBr)(cm^{-1}): 3071 (vw), 2957 (s), 2899 (s), 1940 (vs), 1933 (vs), 1449 (m), 1404 (m), 1381 (m), 1242 (s), 1144 (w), 1024 (m), 843 (vs), 829 (vs), 754 (s), 683 (s); (toluene)(cm^{-1}): ν(C≡C) 1933 (m,sh), 1915 (vs). EI-MS (direct inlet, 200-220 °C, 75 eV): m/z 565(M^+, 0.6%), 526(9), 332(100), 330(25), 328(10), 209(9), 83(38), 39(K^+; 9). ESR (toluene, 23 °C): $g = 1.9914$, $\Delta H = 4$ G, $a_{Zr} = 18.6$ G; (-130 °C): $g_1 = 2.0004$, $g_2 = 1.9915$, $g_3 = 1.9836$, $g_{av} = 1.992$; (MTHF, 23 °C): $g = 1.9907$, $\Delta H = 4$ G, $a_{Zr} = 19.3$ G; (-140 °C): $g_1 = 1.9993$, $g_2 = 1.9913$, $g_3 = 1.9848$, $g_{av} = 1.992$.

2.5. Crystallography

A pale yellow crystal fragment of **1** and a dark green crystal of **2** were mounted into Lindemann glass capillaries in a glovebox (mBraun Labmaster 130) under purified nitrogen and sealed with wax. Diffraction data were measured on a Philips PW 1100 four-circle

Table 2
Atom coordinates and equivalent isotropic temperature factors for non-hydrogen atoms in **1**

Atom	x	y	z	U_{eq} (Å^2)
Zr	0.3225(1)	−0.0864(1)	0.2165(1)	0.048(1)
Si(1)	0.0351(2)	0.1328(1)	0.2584(1)	0.077(1)
Si(2)	0.6424(2)	−0.1058(1)	0.4860(1)	0.078(1)
C(1)	0.2014(4)	0.0056(2)	0.2415(3)	0.061(2)
C(2)	0.1357(4)	0.0560(2)	0.2516(3)	0.066(3)
C(3)	−0.0608(8)	0.1409(4)	0.1573(5)	0.156(7)
C(4)	0.1404(7)	0.2089(3)	0.2715(5)	0.137(6)
C(5)	−0.0733(8)	0.1250(4)	0.3501(5)	0.151(7)
C(6)	0.4576(5)	−0.0891(2)	0.3308(3)	0.070(3)
C(7)	0.5304(5)	−0.0937(2)	0.3934(3)	0.075(3)
C(8)	0.7329(7)	−0.1873(3)	0.4659(4)	0.118(5)
C(9)	0.7558(6)	−0.0323(3)	0.4941(4)	0.112(5)
C(10)	0.5460(6)	−0.1124(3)	0.5854(4)	0.109(5)
C(11)	0.3544(5)	−0.0258(3)	0.0745(3)	0.075(3)
C(111)	0.2442(7)	0.0093(4)	0.0260(4)	0.145(7)
C(12)	0.4434(6)	0.0047(3)	0.1303(3)	0.080(3)
C(121)	0.4435(7)	0.0803(3)	0.1519(5)	0.172(8)
C(13)	0.5351(5)	−0.0414(4)	0.1570(4)	0.098(4)
C(131)	0.6553(6)	−0.0224(6)	0.2089(5)	0.23(1)
C(14)	0.5046(8)	−0.1034(4)	0.1171(5)	0.112(5)
C(141)	0.586(1)	−0.1669(5)	0.1218(8)	0.33(2)
C(15)	0.3920(8)	−0.0938(3)	0.0662(4)	0.100(4)
C(16)	0.1276(6)	−0.1564(3)	0.1771(4)	0.093(4)
C(161)	0.0384(8)	−0.1368(5)	0.1010(6)	0.22(1)
C(17)	0.1072(5)	−0.1383(2)	0.2614(4)	0.079(3)
C(171)	−0.0080(6)	−0.0993(3)	0.2936(7)	0.172(8)
C(18)	0.2018(5)	−0.1700(2)	0.3139(3)	0.073(3)
C(181)	0.2079(8)	−0.1678(4)	0.4109(3)	0.147(6)
C(19)	0.2811(5)	−0.2088(2)	0.2607(4)	0.078(3)
C(191)	0.3892(7)	−0.2564(3)	0.2897(6)	0.159(7)
C(20)	0.2340(6)	−0.2000(3)	0.1773(4)	0.090(4)

Table 3
Atom coordinates and equivalent isotropic temperature factors for non-hydrogen atoms in **2**

Atom	*x*	*y*	*z*	U_{eq} (Å^2)
Zr	0.3801(1)	0.1290(1)	0.2989(1)	0.038(1)
K	0.7706(1)	0.1448(1)	0.1981(1)	0.060(1)
Si(1)	0.7681(2)	0.5319(1)	0.2632(1)	0.060(1)
Si(2)	0.4088(2)	−0.2272(1)	0.0561(1)	0.059(1)
C(1)	0.5671(5)	0.2878(4)	0.2766(2)	0.046(2)
C(2)	0.6608(5)	0.3788(4)	0.2667(3)	0.053(2)
C(3)	0.5976(8)	0.6021(5)	0.2399(5)	0.125(4)
C(4)	0.910(1)	0.5266(6)	0.1905(4)	0.126(4)
C(5)	0.9064(8)	0.6271(5)	0.3604(3)	0.105(3)
C(6)	0.4324(5)	−0.0130(4)	0.1982(2)	0.048(2)
C(7)	0.4471(6)	−0.0934(4)	0.1423(3)	0.056(2)
C(8)	0.2321(8)	−0.3571(5)	0.0615(4)	0.106(3)
C(9)	0.3431(8)	−0.1870(5)	−0.0331(3)	0.085(3)
C(10)	0.6066(8)	−0.2774(5)	0.0445(3)	0.098(3)
C(11)	0.1652(5)	0.2483(4)	0.2919(3)	0.050(2)
C(111)	0.2104(7)	0.3821(4)	0.3403(3)	0.082(3)
C(12)	0.1741(5)	0.2025(4)	0.2121(3)	0.051(2)
C(121)	0.2292(6)	0.2787(5)	0.1597(3)	0.081(3)
C(13)	0.1065(5)	0.0732(4)	0.1869(2)	0.051(2)
C(131)	0.0770(7)	−0.0096(5)	0.1041(3)	0.084(3)
C(14)	0.0534(5)	0.0354(4)	0.2501(3)	0.053(2)
C(141)	−0.0393(7)	−0.0926(5)	0.2473(3)	0.088(3)
C(15)	0.0899(5)	0.1452(4)	0.3153(3)	0.053(2)
C(16)	0.4652(8)	0.0026(4)	0.3780(3)	0.067(2)
C(161)	0.417(1)	−0.1345(5)	0.3469(4)	0.141(5)
C(17)	0.3758(6)	0.0717(5)	0.4236(3)	0.065(2)
C(171)	0.2156(7)	0.0196(7)	0.4537(3)	0.111(4)
C(18)	0.4749(7)	0.1967(4)	0.4477(2)	0.060(2)
C(181)	0.4318(9)	0.3036(6)	0.5023(3)	0.113(4)
C(19)	0.6283(6)	0.2051(5)	0.4189(3)	0.065(2)
C(191)	0.7839(8)	0.3186(6)	0.4401(3)	0.124(4)
C(20)	0.6212(7)	0.0873(6)	0.3748(3)	0.070(3)

diffractometer at room temperature using graphite-monochromated Mo Kα radiation. The intensity data were collected by 2θ–ω scans. The structures were solved by Patterson and Fourier methods which revealed the locations of the non-hydrogen atoms. Their atomic coordinates and anisotropic thermal parameters were refined using the SHELX-76 program [13]. The final refinements were performed by the full-matrix least squares method on all unique F_o^2 data using the SHELXL-93 program [14]. The hydrogen atom contributions were included using a riding model. The PC ULM package [13] was used for the further calculations. Crystal data, details of data collections and refinement are given in Table 1. Atomic coordinates for **1** and **2** are listed in Tables 2 and 3 respectively.

3. Results and discussion

3.1. Synthesis and properties of compound 2

The zirconium(III) tweezer complex, potassium bis(η^5-tetramethylcyclopentadienyl)bis(η^1-trimethyl-silylethynyl)zirconocenate (**2**), was obtained in high yield by the reduction of bis(tetramethylcyclopentadienyl)bis(trimethylsilylethynyl)zirconium(IV) (**1**) with potassium in toluene (Scheme 1). Freshly cut pieces of the potassium metal were used in a large excess as the further reaction of **2** with the metal was not observed overnight. The starting compound **1** was obtained by the reaction of the zirconocene dichloride $(C_5HMe_4)_2ZrCl_2$ with 2 equiv. of LiC≡CSiMe$_3$, following the procedures previously used for obtaining zirconocene [15] or titanocene diacetylides [12]. The crude product contained a paramagnetic impurity which was largely removed only after cumbersome crystallizations from hexane. For the synthesis of **2**, however, a crude **1** can be used since the impurity persists after the reduction with potassium and is removed from the less soluble compound **2** by washing with hexane.

The procedure for preparing **2** is analogous to that originally used to obtain titanocene(III)-alkali metal tweezer complexes [16]. In the zirconocene chemistry, a similar electron transfer reaction probably took place in the reactions of zirconocene diacetylides with the [Cp′$_2$Zr(II)] [15,17,18] or [Ni(PPh$_3$)$_2$] [19] species, implying the transient formation of zirconocene(III) tweezer complexes with embedded transition metals Zr(III) or Ni(I). The final products, however, contained two (μ-η^1:η^2-C≡CR) ligands σ-bonded to each of the metal centres. The zirconocene(IV) tweezer complexes with embedded transition metals are so far unknown, although in the titanocene series a large number of such complexes was reported [20] and hafnocene complexes are also known [21].

Compound **2** is paramagnetic and affords the ESR spectrum consisting of a strong central singlet at $g = 1.9914$ and a weaker sextuplet of equally intense lines. The latter indicates the coupling to the ^{91}Zr nucleus ($I_N = 5/2$, natural abundance 11.23%). The low value of $a_{Zr} = 18.6$ G and the high value of g-factor compared to most of the neutral Zr(III) species [1] indicate a low occupancy of the d-orbital by the unpaired electron. This is also compatible with a low anisotropy of g-tensor in frozen toluene glass. Amongst the alkyl and hydrido zirconocenate complexes the ESR parameters of **2** fall into the medium region: the alkali metal dihydridozirconocenates exert $g \geq 1.992$ and $a_{Zr} \leq 15$ G [1,22] whilst the dialkyl complexes have $g \leq 1.990$ and $a_{Zr} \geq 17$ G [1,23]. The UV-vis spectrum shows a weak absorp-

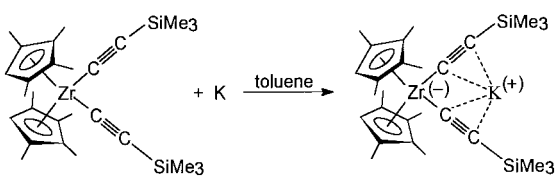

Scheme 1.

tion shoulder whose intensity increases from 800 nm to 580 nm, a pair of strong absorption bands at 440 and 383 nm and a set of sharp bands occurring at 315 nm and shorter wavelengths. Judging from relative intensities, the weak, long-wavelength absorption belongs to a d-d transition and the two strong absorption bands are due to Zr-acetylide charge transfer transitions. All these bands were also observed in analogous titanium tweezer complexes [16]. An extremely small linewidth of the short-wavelength absorption bands at $\lambda_{max} \leq 315$ nm indicates the vibronic structure of an electronic transition, probably involving the orbitals largely confined to the acetylide ligands. Similarly, the electronic transitions of the 4,5-diazafluorene anion displaying the vibronic structure shifted to longer wavelengths upon coordination to titanocene moieties with the preservation of the vibronic structure [24]. The absence of such vibronic features in the same spectral region of the titanium tweezer complexes [16] implies that Zr(III) induces a stronger shift to longer wavelengths of the above-mentioned electronic transition than Ti(III). The infrared spectrum of **2** in KBr pellet is characterized by intense ν(C≡C) vibration bands at 1940 cm^{-1} and at 1933 cm^{-1}. The observed splitting of the band is probably due to the coupling of the acetylide arms via the potassium cation. Compared to the wavenumber of the ν(C≡C) vibration in **1** at 2022 cm^{-1}, the average shift of 90 cm^{-1} is connected with binding of the potassium cation in a π-bonding position between the acetylide tweezer arms as revealed by X-ray single crystal analysis (vide infra). The ν(C≡C) vibrations in the titanium compounds $(\eta^5\text{-}C_5HMe_4)_2Ti(\eta^1\text{-}C{\equiv}CSiMe_3)_2$ (2017 cm^{-1}) and $[(\eta^5\text{-}C_5HMe_4)_2Ti(\eta^1\text{-}C{\equiv}CSiMe_3)_2]^-K^+$ (**3**) differ by only 80 cm^{-1} [16], and this shows that the potassium cation is more strongly bonded in **2** than in **3**. The EI-MS spectrum of **2** showed the molecular peak M^+ with a 0.6% intensity and the main fragment ions $[M\text{-}K]^+$ (9%), $[(C_5HMe_4)_2Zr]^+$ (100%), and $[K]^+$ (9%). This fragmentation pattern does not differ from that of the Ti tweezer complexes [16].

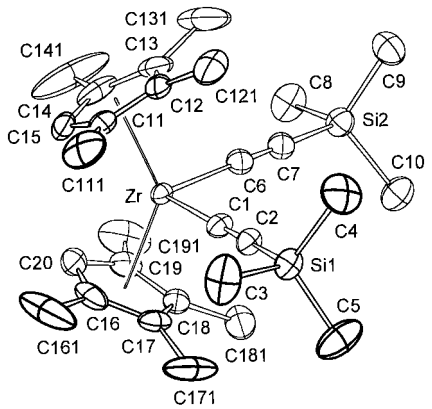

Fig. 1. ORTEP diagram of **1** with thermal ellipsoids drawn at 30% probability level and the atom numbering scheme.

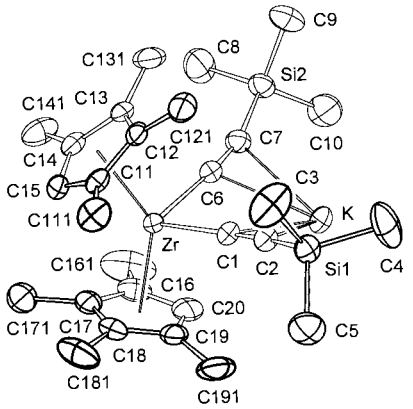

Fig. 2. ORTEP diagram of **2** with thermal ellipsoids drawn at 30% probability level and the atom numbering scheme.

Compound **2** dissolves easily in THF or MTHF; however, evaporation under vacuum at room temperature removes the solvent completely. Surprisingly, the Li^+ cation embedded in similar tweezer complexes coordinates one or two THF molecules even in the solid state, e.g. in $(C_5Me_5)_2Y(C{\equiv}CCMe_3)_2Li(THF)$ [25] and $[(C_5HMe_4)_2Ti(C{\equiv}CC{\equiv}SiMe_3)_2]^-[Li(THF)_2]^+$ [26]. The decreasing tendency to coordinate THF on going from Li to Cs was observed in the series of complexes $[(C_5HMe_4)_2Ti(C{\equiv}SiMe_3)_2]^-[M(THF)_n]^+$ where the complexes for M = K and Cs lost all THF at room temperature [16].

3.2. Crystal structures of compounds *1* and *2*

The bent sandwich zirconocene structures of the tweezer complex **2** and its precursor **1** are both crystallographically asymmetrical. Compound **1** crystallizing in a monoclinic space group has its molecules which are symmetrical around the two-fold rotation axis placed in general positions. ORTEP drawings of **1** and **2** with atom numbering schemes are shown in Figs. 1 and 2 respectively. Selected bond lengths and bond angles for **1** and **2** are given in Table 4. In order to facilitate the comparison with the structure of the closely related complex $[(\eta^5\text{-}C_5HMe_4)_2Ti(\eta^1\text{-}C{\equiv}CSiMe_3)_2]^-K^+$ (**3**) [16] the relevant data for **3** are also included.

The geometrical parameters of compound **1** are very similar to those of dipropynylzirconocene $(C_5H_5)_2Zr(C{\equiv}CMe)_2$ (**4**) [15]. The presence of methyl substituents at the C_5HMe_4 ligand leads to a slightly longer Zr-CE (CE denotes the centroid of the cyclopentadienyl ligand) distance in **1** (av. 2.228 Å) compared to 2.211 Å in **4**, whereas the Zr-C_α distance is slightly shorter (av. 2.225 Å vs. 2.249 Å). The same reason is responsible for a slightly larger CE(1)-Zr-CE(2) angle

Table 4
Selected interatomic distances (Å) and bond angles (deg) for **1** and **2** and for the titanium compound **3**[a]

	1	2	3
Interatomic distances			
Zr–C(1)	2.227(4)	2.264(4)	2.149(4)
Zr–C(6)	2.223(5)	2.279(4)	2.142(4)
C(1)–C(2)	1.206(6)	1.225(6)	1.122(8)
C(6)–C(7)	1.213(7)	1.226(6)	1.231(5)
Si(1)–C(2)	1.827(5)	1.827(5)	1.821(4)
Si(2)–C(7)	1.831(5)	1.825(5)	1.812(4)
K–C(1)	—	2.868(4)	2.946(4)
K–C(6)	—	2.896(4)	2.949(4)
K–C(2)	—	3.105(5)	3.021(4)
K–C(7)	—	3.147(5)	2.961(4)
Zr–C(11)	2.532(5)	2.512(4)	2.399(5)
Zr–C(16)	2.488(6)	2.502(5)	2.422(5)
Zr–C(12)	2.569(5)	2.621(5)	2.528(5)
Zr–C(17)	2.552(5)	2.538(5)	2.415(4)
Zr–C(13)	2.557(6)	2.627(4)	2.523(5)
Zr–C(18)	2.569(5)	2.554(5)	2.450(4)
Zr–C(14)	2.485(8)	2.530(4)	2.418(5)
Zr–C(19)	2.524(5)	2.558(5)	2.428(5)
Zr–C(15)	2.464(7)	2.445(4)	2.333(5)
Zr–C(20)	2.466(6)	2.482(6)	2.389(5)
Zr–CE(1)	2.230(6)	2.244(5)	2.126(5)
Zr–CE(2)	2.226(5)	2.229(5)	2.111(5)
Si(1)–C(Me)$_{av}$	1.841(8)	1.847(7)	1.862(7)
Si(2)–C(Me)$_{av}$	1.863(7)	1.857(7)	1.865(7)
Zr–K	—	3.818(1)	4.033(1)
Bond angles			
C(1)–Zr–C(6)	102.7(2)	92.8(2)	90.1(1)
CE(1)–Zr–CE(2)	135.3(2)	137.3(2)	136.9(2)
Zr–C(1)–C(2)	177.4(4)	175.3(4)	174.9(3)
Zr–C(6)–C(7)	177.0(4)	175.2(4)	177.8(3)
Si(1)–C(2)–C(1)	175.9(4)	167.1(4)	167.6(4)
Si(2)–C(7)–C(6)	176.7(4)	165.4(4)	173.5(4)
K–C(1)–C(2)	—	89.3(3)	81.6(3)
K–C(6)–C(7)	—	90.1(3)	78.5(3)
K–C(2)–C(1)	—	67.5(3)	74.7(2)
K–C(7)–C(6)	—	67.0(3)	77.5(3)
ϕ[b]	51.0	46.8	49.6

[a] The data are taken from Ref. [16]; in the description of bonds and angles read Ti instead of Zr.
[b] The angle between the least squares planes of the cyclopentadienyl rings.

in **1** (135.3°) against 132.6° in **4** and a slightly smaller C(1)-Zr-C(6) bite angle of 102.7° in **1** against 103.6° in **4**. The acetylenic bond lengths (C(1)-C(2) and C(6)-C(7) av. 1.210 Å) and the angles Zr-C(1)-C(2) and Zr-C(6)-C(7) (av. 177.2°) are virtually the same in both compounds.

The zirconocene skeleton in **1** shows a regularly staggered conformation of the C_5HMe_4 ligands with the proton-bearing carbon atoms C(15) and C(20) occupying positions of the closest approach of the rings. Such a conformation was previously found in $(C_5HMe_4)_2TiCl$, $(C_5HMe_4)_2TiI$, $(C_5HMe_4)_2TiCl_2$ [27], $(C_5HMe_4)_2Ti[\eta^2\text{-}C_2(SiMe_3)_2)$ [28], and in the first Ti(III) tweezer complex $[(\eta^5\text{-}C_5HMe_4)_2Ti(\eta^1\text{-}C{\equiv}CSiMe_3)_2]^-[Mg(THF)Cl]^+$ [29]. The less sterically congested $(C_5HMe_4)_2ZrCl_2$, however, adopts the eclipsed conformation of the rings [30]. All these structures have the ring planes inclined to each other more than would correspond to the perpendicular orientation of the M-CE (M = Ti, Zr) vector to the ring plane. The sum of angles CE-M-CE and the angle ϕ between the ring planes in these compounds exceeds 180°, and hence the ring slippage angle α is correspondingly lower than 90°. In **1**, the angle ϕ 51° corresponds to $\alpha = 86.85°$.

The conformation of the C_5HMe_4 ligands in **2** is different. The CE(1) ring (C(11)-C(15)) points by the proton bearing carbon atom C(15) towards the top of angle ϕ, whereas the CE(2) ring is directed by the analogous carbon atom C(20) towards the potassium atom side in a slightly staggered conformation of the rings (Fig. 2). The CE(1) ring plane is inclined by the C(15) atom to the Zr atom, as in **1**; however, the reversely orientated CE(2) ring is approximately perpendicular to the Zr-CE(2) vector. As a result, angle ϕ 46.8° is smaller by 4.2° than that in **1**.

The planes defined by CE(1), Zr, and CE(2) and by the C(1), Zr, and C(6) atoms are mutually perpendicular within 0.9° for both **1** and **2**. The C(1)-Zr-C(2) bite angle in **2** (92.8(2)°) is by about 10° larger than that in **2** (Table 4). In contrast to **1**, where the tweezer arms lie close to the bite angle plane, the tweezer part of compound **2** is considerably distorted. The potassium atom is located between the acetylide arms; however, it is placed 1.13 Å below the bite angle plane. Consequently, the two acetylide arms are bent towards the opposite side of this plane (C(2) -0.049 Å, C(7) -0.076 Å, Si(1) -0.287 Å and Si(2) -0.498 Å). The Zr-C(1)-C(2) angle and Zr-C(6)-C(7) angles 175.2° and 175.3° in **2** are smaller by about 2° than those in **1**, and the acetylide arms are much more bent (C(1)-C(2)-Si(1) and C(6)-C(7)-Si(2) angles 167.1° and 165.4°) than in **1** (corresponding angles 175.9° and 176.7°). The potassium atom is much closer to the inner acetylide carbon atoms than to the outer ones. However, the K-C(1) 2.868(4) Å and K-C(6) 2.896(4) Å distances are larger than the sum of covalent radii of both the atoms (2.03 Å and 0.77 Å), and thus the ionic nature of the potassium binding is to be assumed. The K-C distances towards the outer acetylide carbon atoms are 3.13 Å on the average. The Zr-K distance of 3.818(1) Å is shorter by 0.215 Å than the Ti-K distance in **3** (4.033(1) Å). Since the covalent radius of Zr is 1.45 Å and that of Ti only 1.32 Å the effective difference is even more pronounced. The shorter Zr-K distance apparently reflects both a larger bite angle and an overall stronger interaction of the tweezer arms with the potassium cation, as is demonstrated by the larger red shift of the ν(C≡C) vibration and by the electronic transition showing the vibronic structure (vide supra).

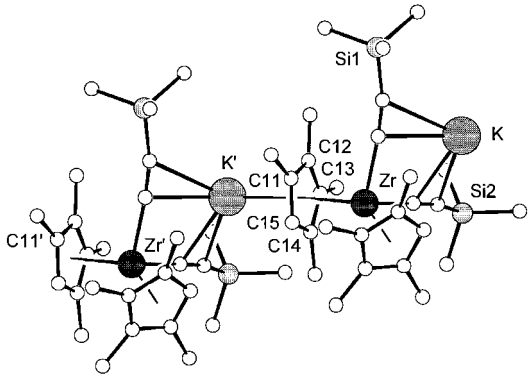

Fig. 3. PLUTO diagram showing the polymeric structure of **2**.

The conformation of the cyclopentadienyl ligands and the distortion of the molecule **2** is probably brought about by the polymeric nature of the compound in the solid state, as is shown on a dimer fragment of the molecular chain (Fig. 3). The strongest intermolecular interaction occurs between the potassium cation and the cyclopentadienyl ring CE(1)′ of an adjacent molecule. This mode of intermolecular interaction has also been observed in the titanium analogue **3** [16] and in $[(C_5Me_5)_2Sm(\eta^1\text{-}C{\equiv}CPh)_2K]_n$ [31]. The intermolecular distances and angles for **1** and **3** are compared in Table 5. The distances from K^+ to the adjacent ring indicate that the π-like interaction between K^+ and the C_5HMe_4 ring is much stronger in **2** than in **3**. It is also expressed in the nearly linear arrangement of K′, CE(1) and Zr points. The zig-zag structure of the polymeric chain resembles that in **3** as the angle K-M-K′ (M = Zr or Ti) is nearly equal for both the metals and the difference in the M-CE(1)-K′ angle is compensated by the opposite difference in the angle M-K′-M′. A stronger interaction between the potassium cation and the C_5HMe_4 ring in **2** thus may induce a larger deviation of the potassium cation from the plane of bite angle than in **3**. Further investigation into the structures of modified tweezer complexes of this type is under way.

Table 5
The comparison of intermolecular interactions in **2**[a] and **3**

	2	**3**[b]
Interatomic distances		
K′CE(1)	2.871(5)	3.186(5)
K′–C_{av}(C(11)–C(15))	3.114(5)	3.394(5)
Angles		
K′–Zr–K	128.9(1)	128.2(2)
Zr–K′–Zr′	128.9(1)	151.7(1)
Zr–CE(1)–K′	175.4(2)	155.7(1)

[a] Atom labeling is as given in Fig. 2.
[b] The data are taken from Ref. [16]; in the description of angles read Ti instead of Zr.

4. Supplementary material

Listings of atomic coordinates, bond lengths and angles and thermal parameters have been deposited at the Cambridge Crystallographic Data Centre. These, together with lists of observed and calculated structure factors and further details of the structure determination, are available from the authors (J.H.).

Acknowledgements

This work was supported by the Grant Agency of the Czech Republic (Grant No. 203/96/0948), and by the Volkswagen Stiftung. The Grant Agency of the Czech Republic (grant No. 203/96/0111) sponsored an access to Cambridge Structure Data Base. The authors thank Mrs. G. Dörfner for the EDX measurements.

References

[1] E.J. Ryan, in: E.W. Abel, F.G.A. Stone, G. Wilkinson (Eds.), Comprehensive Organometallic Chemistry II, vol. 4, M.F. Lappert (Ed.), Elsevier, 1995, Chapter 8, pp. 465-481.
[2] I.F. Urazowski, V.I. Ponomaryev, I.E. Nifant'ev, D.A. Lemenovskii, J. Organomet. Chem. 368 (1989) 287.
[3] R.D. Rogers, J.H. Teuben, J. Organomet. Chem. 359 (1984) 41.
[4] H. Brand, J. Arnold, Angew. Chem. Int. Ed. Engl. 34 (1994) 53.
[5] M.D. Fryzuk, M. Mylvaganam, M.J. Zaworotko, L.R. MacGillivray, Polyhedron 15 (1996) 689.
[6] R. Gyepes, J. Hiller, U. Thewalt, M. Polášek, P. Šindelář, K. Mach, J. Organomet. Chem. 516 (1996) 177 and references cited therein.
[7] M. Bénard, M.-M. Rohmer, J. Am. Chem. Soc. 114 (1992) 4785; Organometallics 10 (1991) 157.
[8] M.J.S. Gynane, J. Jeffery, M.F. Lappert, J. Chem. Soc. Chem. Commun. (1978) 34.
[9] P.B. Hitchcock, M.F. Lappert, G.A. Lawless, H. Olivier, E.J. Ryan, J. Chem. Soc. Chem. Commun. (1992) 474.
[10] H. Antropiusová, A. Dosedlová, V. Hanuš, K. Mach, Transition Met. Chem. 6 (1981) 90.
[11] P. Courtot, V. Labed, R. Pichon, J.Y. Salaün, J. Organomet. Chem. 359 (1989) C9. J. Hiller, U. Thewalt, M. Polášek, L. Petrusová, V. Varga, P. Sedmera, K. Mach, Organometallics 15 (1996) 3752.
[12] H. Lang, D. Seyferth, Z. Naturforsch. Teil B: 45 (1990) 212.
[13] R. Bruggemann, T. Debaerdemaeker, B. Müller, G. Schmid, U. Thewalt, ULM Programmsystem, 1. Jahrestagung der Deutschen Gesellschaft für Kristallografie, Mainz, 9-12 June, 1992, Abstr., p. 33 (includes G.M. Sheldrick, SHELX-76 Program for Crystal Structure Determination, University of Cambridge, Cambridge, UK, 1976).
[14] G.M. Sheldrick, SHELXL-93 Program for Crystal Structure Refinement, University of Göttingen, Germany, 1993.
[15] G. Erker, W. Frömberg, R. Benn, R. Mynott, K. Angermund, C. Krüger, Organometallics 8 (1989) 911.
[16] V. Varga, J. Hiller, M. Polášek, U. Thewalt, K. Mach, J. Organomet. Chem. 515 (1996) 57.

[17] U. Rosenthal, A. Ohff, W. Baumann, R. Kempe, A. Tillack, V.V. Burlakov, Organometallics 13 (1994) 2903.
[18] H. Lang, S. Blau, B. Nuber, L. Zsolnai, Organometallics 14 (1995) 3216.
[19] U. Rosenthal, S. Pulst, P. Arndt, A. Ohff, A. Tillack, W. Baumann, R. Kempe, V.V. Burlakov, Organometallics 14 (1995) 2961.
[20] H. Lang, K. Köhler, L. Zsolnai, Chem. Commun. (1996) 2043. H. Lang, K. Köhler, S. Blau, Coord. Chem. Rev. 143 (1995) 113 and references cited therein.
[21] H. Lang, M. Herres, L. Zsolnai, Bull. Chem. Soc. Jpn. 66 (1993) 429. H. Lang, M. Herres, W. Imhof, J. Organomet. Chem. 465 (1994) 283.
[22] A.-M. Larsonneur, R. Choukroun, J. Jaud, Organometallics 12 (1993) 3216.
[23] M.F. Lappert, C.J. Pickett, P.I. Riley, P.I.W. Yarrow, J. Chem. Soc. Dalton Trans. (1981) 805.
[24] P.T. Witte, R. Klein, H. Kooijman, A.L. Spek, M. Polášek, V. Varga, K. Mach, J. Organomet. Chem. 519 (1996) 195.
[25] W.J. Evans, D.K. Drummond, T.P. Hanusa, J.M. Olofson, J. Organomet. Chem. 376 (1989) 311.
[26] V. Varga, K. Mach, J. Hiller, U. Thewalt, J. Organomet. Chem. 506 (1996) 109.
[27] S.I. Troyanov, V.B. Rybakov, U. Thewalt, V. Varga, K. Mach, J. Organomet. Chem. 447 (1993) 221.
[28] V. Varga, K. Mach, M. Polášek, P. Sedmera, J. Hiller, U. Thewalt, S.I. Troyanov, J. Organomet. Chem. 506 (1996) 241.
[29] S.I. Troyanov, V. Varga, K. Mach, Organometallics 12 (1993) 2820.
[30] C. Janiak, U. Versteeg, K.C.H. Lange, R. Weimann, E. Hahn, J. Organomet. Chem. 501 (1995) 219.
[31] W.J. Evans, R.A. Keyer, J.W. Ziller, Organometallics 12 (1993) 2618.